Editors' Suggestion

Nucleation of ripplocations through atomistic modeling of surface nanoindentation in graphite

D. Freiberg,[1] M. W. Barsoum,[1] and G. J. Tucker[1,2]
[1]*Department of Materials Science and Engineering, Drexel University, Philadelphia, Pennsylvania 19104, USA*
[2]*Department of Mechanical Engineering, Colorado School of Mines, Golden, Colorado 80401, USA*

(Received 24 October 2017; published 4 May 2018)

In this work, we study the nucleation and subsequent evolution behavior of ripplocations – a newly proposed strain accommodating defect in layered materials where one, or more, layers buckle orthogonally to the layers – using atomistic modeling of graphite. To that effect, we model the response to cylindrical indenters with radii R of 50, 100, and 250 nm, loaded edge-on into graphite layers and the strain gradient effects beneath the indenter are quantified. We show that the response is initially elastic followed by ripplocation nucleation, and growth of multiple fully reversible ripplocation boundaries below the indenter. In the elastic region, the stress is found to be a function of indentation volume; beyond the elastic regime, the interlayer strain gradient emerges as paramount in the onset of ripplocation nucleation and subsequent in-plane stress relaxation. Furthermore, ripplocation boundaries that nucleate from the alignment of ripplocations on adjacent layers are exceedingly nonlocal and propagate, wavelike, away from the indented surface. This work not only provides a critical understanding of the mechanistic underpinnings of the deformation of layered solids and formation of kink boundaries, but also provides a more complete description of the nucleation mechanics of ripplocations and their strain field dependence.

DOI: 10.1103/PhysRevMaterials.2.053602

I. INTRODUCTION

Layered solids, as diverse as graphite, mica, polymer composites, and wood, among many others, deform differently than their nonlayered counterparts. In these solids—defined herein as solids in which the deformation is, at least initially, confined to two dimensions (2D)—compressing the layers edge-on causes out-of-plane buckling. This buckling, in turn, results in kink bands. The latter have been extensively studied in the geological [1–6], ice [7], composites [8–10], and metallurgical [11–14] literature, again among many others. In short, any field wherein buckling and kink band formation have been observed, they have been modeled and experimentally studied.

Along the same lines, it has long been appreciated that for solids to plastically deform, defects must be present. Crucially, when the literature on the deformation of crystalline, layered solids is reviewed, it is clear that—implicitly or explicitly—the micromechanism responsible for their deformation is, in all cases, assumed to be the *basal dislocation* (BD) [1–5,15,16]. Very recently, we made a strong case that the conventional wisdom—with the notable exception of most metals and materials that twin—is incorrect and/or incomplete [17].

In early 2015, Kushima *et al.* [18] presented evidence for a new micromechanism they termed a *ripplocation.* Ripplocations were defined as surface ripples operative during the deformation of 2D, weakly bonded, van der Waals solids [18]. We extended their initial idea to *all* layered solids and showed—by combining atomistic modeling on graphite with nanoindentation experiments on the layered ternary carbide, Ti_3SiC_2—that bulk ripplocation (BR) formation is essentially an atomic-scale buckling phenomenon. In other words, we showed that BRs are not restricted to van der Waals solids, as initially postulated, but occur in bulk and thus are not necessarily restricted to surfaces or near surfaces. Since we have already established this idea, henceforth we will simply refer to a BR as a ripplocation. We also showed that unlike dislocations, ripplocations have no Burgers vector or polarities [19]. Their energies depend on the amount of "excess" material that needs to be accommodated, or degree of in-plane compressive strain and strain accommodated in the surrounding layers. In graphite, ripplocations were shown to be attracted to other ripplocations, both within the same layer and on adjacent layers, with the latter resulting in what we originally termed kink boundaries (KBs), but are now calling ripplocation boundaries or RBs. The critical distinction being that the latter is *fully reversible*; the former are not. When the radii of curvatures of the RBs are no longer sustainable, they transform to the ubiquitous and well-established KBs.

Our initial atomistic calculations on graphite also showed that the RBs are quite mobile indeed, even at 10 K. Lastly, we made the case that ripplocations are a topological imperative, as they allow atomic layers to glide relative to each other without breaking the all-important in-plane bonds [19]. Previously we also showed that when single Ti_3SiC_2 grains were indented normal to the basal planes, the response was radically different than when they were loaded edge-on [20]. For example, the friction stress measured was almost three times lower when the basal planes were loaded edge-on as when they were loaded normal to the basal planes. Furthermore, our molecular dynamics (MD) simulations on graphite at 10 K faithfully reproduced many features observed below the indenter in Ti_3SiC_2.

Collectively, these early findings suggest that ripplocations are critical in governing the deformation response of layered solids, and therefore a more complete understanding of ripplocation-driven deformation is needed to improve predictions of the mechanical behavior of layered solids. As such, this work importantly elucidates the influence of local strain fields on ripplocation nucleation and their evolution to form larger-scale RBs in graphite using atomistic modeling.

The findings form a critical component for future modeling efforts and provide insight into the multitude of layered solids deforming through ripplocations.

II. COMPUTATIONAL METHODOLOGY

A. Atomistic modeling approach

As in our previous work, the atomistic modeling software LAMMPS [21] and an AIREBO potential were used to simulate surface nanoindentation of graphite using a quasistatic loading approach [19]. The simulation cell consisted of 400 layers, with approximately 2 million atoms. Periodic boundary conditions, in both the y and z directions, were employed. (Coordinate system is shown in bottom right of Fig. 1(a)). The atoms in the bottom 30 Å in the x direction were held fixed in all directions during indentation; the atoms near the top surface were free. Quasistatic loading of the graphite structure was performed by alternating between indentation steps and full energy minimization of the atoms. The cylindrical indenter was modeled as a repulsive potential spanning the entire y dimension, acting radially away from the center of the indenter on any atom within a distance less than the prescribed indenter radius R. The indenter was incrementally moved, in the negative x direction, such that the cylinder's axis was parallel to the graphite layers (y direction).

B. Atomic-level stress and strain calculations

To quantify the compressive strain per layer, we leverage a set of microscale kinematic metrics that have been shown to provide valuable insight into nanoscale mechanisms and strain/deformation fields to help analyze the resulting atomistic simulation data by Tucker *et al.* [22,23]. The strain tensor of each atom is calculated at every indentation step based on the deformation of surrounding atoms. Then, the total layer strain is found by summing the strain of each atom, within the layer, and, lastly, normalizing per atom.

The stress of the system was calculated by summing all atomic stresses (according to the virial definition per atom) and normalizing by the *total* number of atoms. Note this definition of stress does *not* capture the effect of different indenter sizes nor does it capture the force on the indenter. However, it does capture the accumulated stress within the system due to indentation.

C. Nanoindentation parameters

Three indenters, with radii R of 50, 100, and 250 nm, were modeled separately. Each indenter was moved a total distance of 12.5 Å in increments of 0.025 Å during each indentation step. Energy minimization of the atoms followed each indentation step to an energy convergence criteria of 1×10^{-8} eV. This criterion defines the energy difference between two successive iterations during minimization. Following each full iteration (indentation step plus energy minimization), a snapshot of the atomic structure—containing different atomic metrics: position, energy, force, stress, and both displacement and strain (relative to the initial structure before indentation)—was output.

III. RESULTS AND DISCUSSION

A. Indentation-induced nucleation of ripplocations

Movies of the atomistic simulations for indenters with $R = 50$ and 250 nm are shown in Supplemental Material [24]. Figures 1(a) and 1(b) show, respectively, views of the indentations at maximum indentation depth of ≈12.5 Å for $R = 50$ and $R = 250$ nm. From these images, it is clear that multiple alternating RBs, of opposite sign, form beneath the indenter due to the self-alignment of ripplocations. The coloring scheme highlights the fact that oppositely signed RBs continue to grow laterally with further indentation as more layers are compressively strained and subsequently buckle, forming additional ripplocations that align with the RBs that are already present, leading to larger RBs. Note the difference in RB magnitude and spacing as a function of R, suggesting an influence of the latter. In other words, *the gradient of indentation-induced strain beneath the indenter to form ripplocations, and thus RBs, is critically important in the nucleation of ripplocations and their evolution with further deformation*.

When the calculated stress in the x direction, σ_{11}, is plotted as a function of indentation depth h for different R values [Fig. 2(a)], it is clear that σ_{11} is initially proportional to the nanoindenter's maximum depth, with proportionality constants that differ for each R, as the total number of layers compressed and the total compression of each layer vary. The maximum stress for R of 250 nm is approximately, $\sigma_{11} \approx 110$ MPa, whereas for R of 50 nm, it is $\sigma_{11} \approx 60$ MPa.

B. Effect of strain gradient on nucleation

At an indentation depth of about 5 Å for the larger 250 nm indenter, layers closest to the center of the indenter (and therefore the most compressed during elastic loading) began to buckle, nucleating ripplocations that led to the formation and propagation of the aforementioned RBs. The critical indentation depth (5 Å) is noted in Fig. 2(a) near the peak of the stress-indentation curve for the 250 nm indenter. For the 50 and 100 nm indenters, the nucleation points—also occurring near the peak stress—appear to be near 6 and 5.5 Å, respectively. Said otherwise, ripplocation nucleation occurs at larger depths with decreasing R. This indicates that for smaller R, the layers directly beneath the indenter can accommodate more *in-plane* compressive strain prior to when ripplocation nucleation (or out-of-plane buckling) occurs to form RBs. This important observation motivated further analysis of the total strain accommodated beneath the indenter.

A convenient way to think about this process is that during elastic loading, the layers directly beneath the indenter's axis are the most compressed and the compressive strain in the surrounding layers is a function of R. With a smaller R, the gradient of compressive strain between neighboring layers is larger than with a larger R. If adjacent graphite layers are more highly strained, nucleation can occur at lower indentation depths (as exhibited in the 250 nm case)—*indicating that the critical in-plane strain in a given layer required for ripplocation nucleation is influenced by the local strain field in adjacent layers*. From our earlier work, we found that there is a critical degree of compressive strain needed for nucleation based on excess material per unit length [19]. However, these results

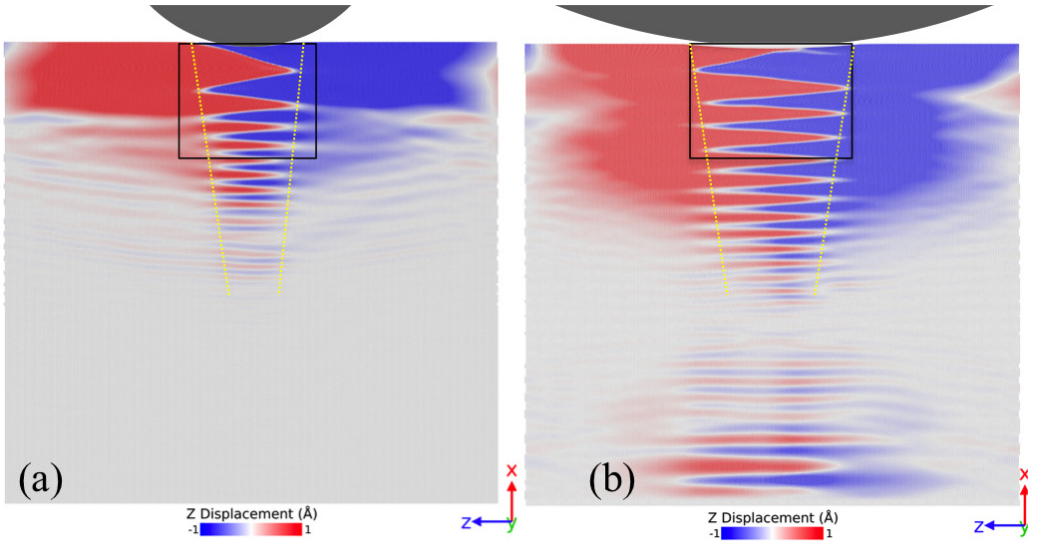

FIG. 1. Atomistic modeling of cylindrical nanoindentation of graphite, edge-on to the layers. Images show atomic displacements in the z direction at an indentation depth of 12.5 Å with (a) 50 nm and (b) 250 nm radius cylindrical indenter with axis parallel to the y direction. Atom coloring corresponds to out-of-plane displacement (z direction). Yellow dotted lines highlight deformed regions comprised of RBs of opposite signs forming across multiple graphite layers. RBs are defined as the locus joining points with the highest curvature in each layer. In this case they are parallel to the surface.

suggest that understanding ripplocation nucleation requires considering the strain state of the surrounding material as well.

C. Normalization by indenter volume

Attempting to better understand this result, Fig. 2(b) plots the same computed indentation stress from the simulations by the indentation volume V_I. The latter is calculated as the overlapping volume between the cylindrical indenter and the rectangular graphite structure as a function of indentation depth and R, assuming

$$V_I = R^2\cos^{-1}\left(\frac{R-h}{R}\right) - (R-h)\sqrt{2Rh-h^2},$$

where h is the indentation depth. A more complete description of this approach is given by Gordon *et al.* [25]. Therefore, at the same h, V_I is greater for a larger R than that for a smaller R. This approach follows from our early hypothesis that for a given h, more layers are being indented when R is larger. When σ_{11} is now plotted as a function of V_I [Fig. 2(b)], the initial response of all R values is identical, confirming the linear elastic nature of this response and the importance of the indented volume. However, beyond the linear elastic regime and upon ripplocation nucleation, the curves diverge substantially. From Fig. 2(a), we know that ripplocation nucleation occurs at lower indentation depths for $R = 250$ nm; however, Fig. 2(b) shows that at this point (labeled II), a significantly larger volume of graphite has been indented, as compared to the two smaller R cases.

This data strongly support the suggested role of strain accommodation in nearby layers and the total stored strain within the indented region on ripplocation nucleation. Otherwise, if only the nucleation of the first ripplocation mattered, all R would induce nucleation at approximately the same indentation depth. However, Fig. 2(b) suggests that ripplocation nucle-

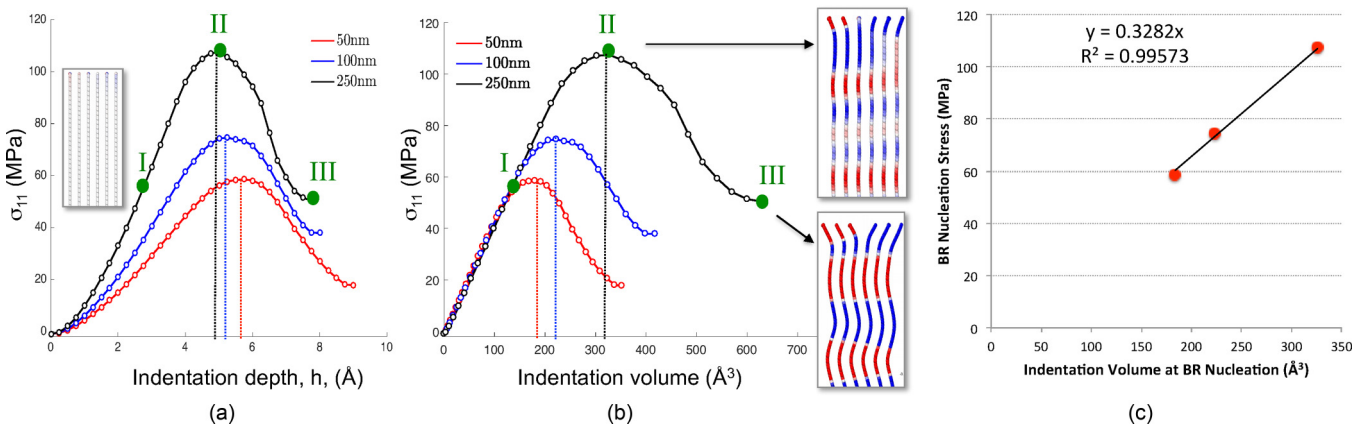

FIG. 2. (a) Dependence of σ_{11} on indentation depth h for cylindrical indenters with R of 250 nm (black), 100 nm (blue), and 50 nm (red). Inset shows configuration at point I. (b) Dependence of σ_{11} on indentation volume. Snapshots of the atomic z displacements, corresponding to points II and III, are shown on the right. (c) Effect of ripplocation nucleation stress on indented volume.

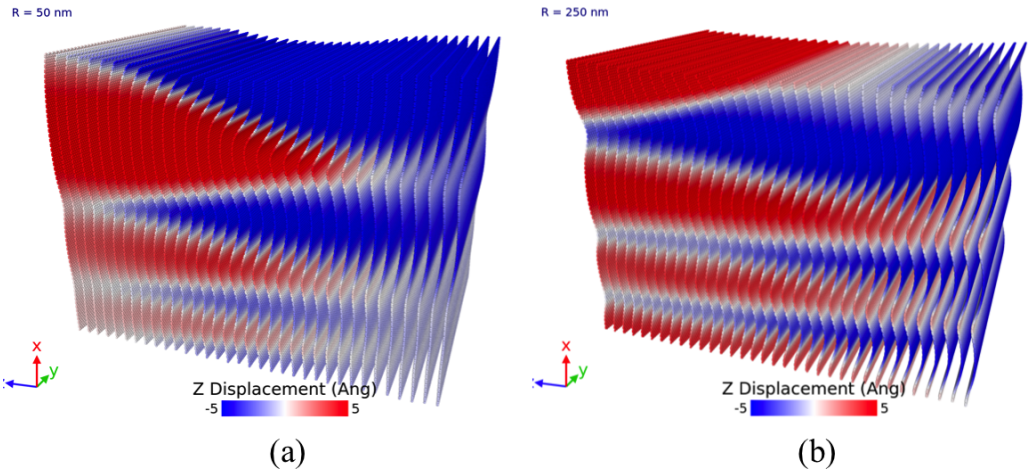

(a) (b)

FIG. 3. The resulting atomic structures after the nucleation of ripplocations and subsequent evolution into RBs for the (a) 50 nm and (b) 250 nm indenter. The structures are close-up views of the including black boxes shown in Fig. 1 directly beneath the indenter, where every one in three atomic layers are included to more clearly show the alignment of ripplocations, as buckling at the atomic scale of the graphite layers, to form oppositely directed RBs.

ation, and subsequent RB formation, should be considered to be a function of *total* strain accommodation, not just indentation depth, and is a strain accommodation mechanism influenced by nonlocal effects.

D. Nucleation strain gradient dependence

As the major aim of our work is to better understand ripplocation nucleation, snapshots of the atomic z displacements at indentation depths of (I) 2.5 Å, (II) 5 Å, and (III) 8 Å are provided in Figs. 2(a) and 2(b) for the $R = 250$ nm simulation, as insets. From these snapshots, it is reasonable to conclude that nucleation corresponds to a point near the maxima of the curves shown in Figs. 2(a) and 2(b), and that further indentation leads to additional ripplocations and the formation of RBs, as observed in Movies 1 and 2 of the Supplemental Material [24]—see detailed discussion below of the movies. This comment notwithstanding, determining the exact nucleation point of the ripplocations is difficult to define. For example, a periodic displacement in the z direction was detectable in the central graphite layer—at an indentation depth of about 1 Å for all R simulated (not shown)—that could be interpreted as the nucleation point, or at an indentation depth just past the nucleation point. Here, we suggest that, operationally, the nucleation point is best defined as *the* point at which the stress is *near* a maximum. Relating the stress at the nucleation point to V_I is provided in Fig. 2(c). A linear fit is also provided for this limited data set that seems to support our hypothesis concerning nonlocal effects on ripplocation nucleation and evolution.

It is paramount here to better appreciate what occurs at the maximum stress. At that point, a redirection of in-plane compressive strain—during which primary bonds are loaded—to orthogonal out-of-plane strain leads to atomic buckling. To those familiar with buckling theory, this is simply confined buckling. What is noteworthy is that this is occurring at the atomic level and is strongly coupled to the gradient of accommodated strain in the nearby layers, as discussed above, and shown in Fig. 3. The strain gradient influence on the formation of RBs from ripplocation alignment, due to R, manifests as varying amplitudes and widths seen in the RBs beneath the indenter, seen in Fig. 3. In our previous study [19], we did not consider strain accommodation in nearby layers. Our revised understanding of the role of strain gradients can only be strengthened by a more quantitative mapping of accumulated compressive strain within the graphite layers during indentation as a function of R and indentation depth. Discussed above, the stress in the elastic region is hypothesized to be a function of indentation volume (or, more precisely, a function of the sum of the indentation depths of each layer), while the ripplocation nucleation depth is hypothesized to be a function of the strain gradient and thus inversely proportional to R.

Figure 4 shows how the compressive strain is distributed in the layers beneath the indenter, as a function of R and h. Strain per atomic layer is provided along the y axis, while the individual layer numbers are on the x axis. In this case, we only consider the strain tensor component in the indentation direction. When the layer strain for the three indenters is displayed for $h = 2.5$ Å, i.e., at a point prior to ripplocation nucleation, it is clear that the layers *directly* beneath the indenter have almost identical compressive strains for all three R values. However, in the surrounding layers, the accommodated compressive strain varies as a function of R. Therefore, not surprisingly, the strain gradient orthogonal to the indentation axis is strongly correlated to R.

Figure 4(b) plots the same variables, but at h of 5 Å, where we know from the simulations that only the layers under the $R = 250$ nm indenter buckled. It follows that the parabolic layer-strain profile [Fig. 2(a)] has only been altered due to ripplocation nucleation for $R = 250$ Å. The compressive strain in nearby layers drops significantly after ripplocation nucleation, indicating the preference to form ripplocations that spontaneously align to form RBs to accommodate the imposed compressive strain. Interestingly, although the peak compressive strain in the layers beneath the indenter (i.e., layer 200) is approximately equal for all R, the stored strain in layers further away from the center line (i.e., more than 20 layers away from the center) deviates substantially, as a function of R.

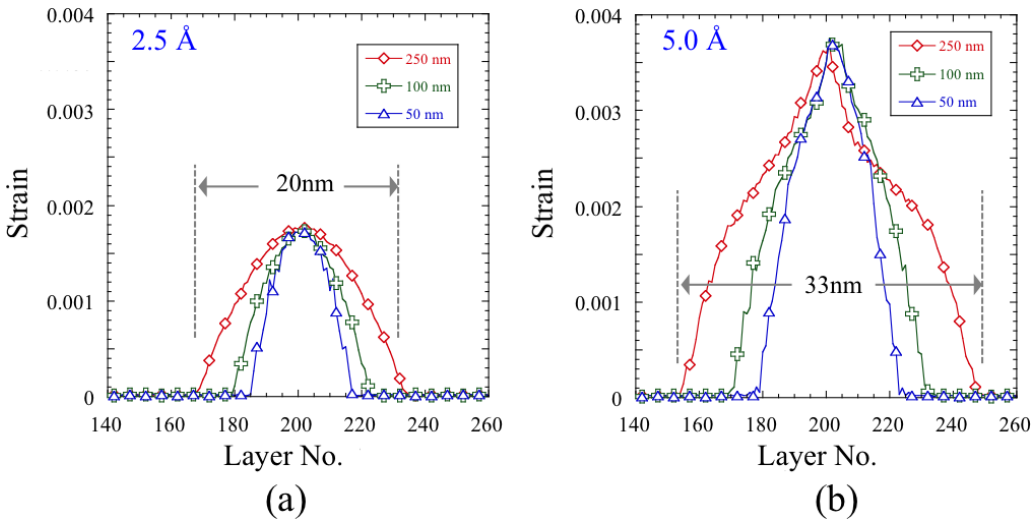

FIG. 4. Functional dependence of compressive strain (along the x axis) on each layer at indentation depths, h, of (a) 2.5 Å and (b) 5 Å, for all three R values. At $h = 2.5$ Å, the strain distribution for each indenter is roughly parabolic, while at 5 Å, a shoulder, which is indicative of ripplocation nucleation, is clearly seen in the 250 nm indenter data, but not for the other two cases—showing the influence of strain gradient and distribution of strain in the layers.

E. Delocalization of deformation

Movie 1 and Movie 2 of the Supplemental Material [24] show the full atomistic simulation of graphite under nanoindentation using, respectively, an R of 50 and 250 nm. The atoms are colored according to their calculated displacement in the z direction (i.e., normal to the graphite layers) relative to the initial undeformed atomic structure. The movies continue until the total indentation depth is 12.5 Å. Initially, the indentation-induced strain is accommodated within the graphite layers, as in-plane compressive strain. Then, when a critical point is reached [Fig. 4(b)], the compressive strain transitions to out-of-plane buckling. This buckling occurs at the atomic scale (Fig. 3). With further indentation and nucleation of additional ripplocations, the ripplocations energetically align with adjacent layers to form RBs of opposite signs that propagate away from the indenter into the material. Notably, the extent of RB formation and evolution during indentation varies between Movie 1 and Movie 2 (Supplemental Material [24]) due to the effect of indenter radius on the strain gradient.

What is most striking about the movies is how, upon the nucleation of ripplocations, spontaneously opposite-signed RBs—which entail the collective motion of multiple layers—are formed. What is also striking is how the extent of deformation is greatly delocalized by the wavelike nature of the RBs. In short, after enough compressive strain has accumulated, it is redistributed by greatly delocalizing it. Said otherwise, the strain is redistributed from expensive in-plane bonds to much cheaper out-of-plane bonds. Lastly, it is crucial to note that like in all of our simulations on graphite the process is fully and spontaneously reversible.

IV. CONCLUSIONS

In conclusion, through atomistic simulations of graphite, indented parallel to the layers by cylindrical nanoindenters with radii of 50, 100, and 250 nm, three distinct regimes were observed. Initially, the response is linear elastic, wherein the stress is proportional to the indentation volume (corresponding well to the sum of the indentation-induced strains of each layer of graphite). This regime is followed by ripplocation nucleation that begins at smaller indentation depths for larger indentation radii. In the third regime, the individual ripplocations self-assemble into RBs of opposite sign that spontaneously spread out along the graphite layers to further lower the system's energy.

Ripplocations nucleate only after a critical number of layers have undergone a critical amount of compressive strain. Thus, ripplocation nucleation in layered solids is fundamentally tied to the strain gradient or to stored compressive in-plane strain in adjacent layers—a nonlocal effect. This insight is critical for understanding RB formation, strain reversibility, and forming predictive approaches for the mechanical behavior of layered solids, where ripplocations are the operative deformation mechanism.

That *all* layered materials when loaded in compression deform by the formation of RBs that ultimately transform to permanent KBs, but not when loaded in tension, is no coincidence. It follows that because ripplocations are totally agnostic to whether the layers being loaded are crystalline or amorphous, the implications and ramifications of our conclusions have broad appeal and indeed will impact all fields of study in which layered solids are deformed, starting with 2D materials, extending to layered polymers and polymer composites, and finally ending at geologic scales. What we present here, in principle, applies over 12 orders of magnitude and should be more thoroughly studied. The fact that insight gained from deforming 400 layers of graphite can shed light on, or could potentially be applicable to, geologic formation is quite remarkable. The simplicity and universality of Nature's solution to the problem of deforming layered materials is truly elegant.

ACKNOWLEDGMENT

This work was supported by the National Science Foundation under Grant No. 1728041.

[1] R. Christoffersen and A. K. Kronenberg, J. Struct. Geol. **15**, 1077 (1993).
[2] A. Kronenberg, S. Kirby, and J. Pinkston, J. Geophys. Res. **95**, 19257 (1990).
[3] V. M. Mares and A. K. Kronenberg, J. Struct. Geol. **15**, 1061 (1993).
[4] I. A. Bell and C. J. Wilson, Tectophysics **78**, 201 (1981).
[5] I. A. Bell, C. J. L. Wilson, A. C. McLaren, and M. A. Etheridge, Tectonophysics **127**, 49 (1986).
[6] R. L. Bell and R. W. Cahn, Proc. Roy. Soc. A **239**, 494 (1957).
[7] M. E. Manley and E. M. Schulson, Philos. Mag. Lett. **75**, 83 (1997).
[8] B. Budiansky, N. A. Fleck, and J. C. Amazigo, J. Mech. Phys. Solids **46**, 1637 (1998).
[9] Q. Yang and B. Cox, Int. J. Fracture **133**, 107 (2005).
[10] N. Fleck, Adv. Appl. Mech. **33**, 43 (1997).
[11] E. Orowan, Nature (London) **149**, 643 (1942).
[12] F. C. Frank and A. N. Stroh, Proc. Phys. Soc. **65**, 811 (1952).
[13] J. J. Gilman, Trans. AIME **6**, 621 (1954).
[14] J. B. Hess and C. S. Barrett, Trans. AIME **185**, 599 (1949).
[15] B. T. Kelly, *Physics of Graphite* (Applied Science, London, 1981).
[16] A. Meike, Am. Mineral. **74**, 780 (1989).
[17] M. W. Barsoum and G. J. Tucker, Scr. Mater. **139**, 166 (2017).
[18] A. Kushima, X. Qian, P. Zhao, S. Zhang, and J. Li, Nano Lett. **15**, 1302 (2015).
[19] J. Gruber, A. Lange, J. Griggs, M. Taheri, G. Tucker, and M. W. Barsoum, Sci. Rep. **6**, 33451 (2016).
[20] J. Griggs, A. Lang, J. Gruber, G. Tucker, M. Taheri, and M. W. Barsoum, Acta Mater. **131**, 141 (2017).
[21] S. Plimpton, J. Comput. Phys. **117**, 1 (1995).
[22] G. J. Tucker and S. M. Foiles, Int. J. Plast. **65**, 191 (2015).
[23] G. J. Tucker, S. Tiwari, J. A. Zimmerman, and D. L. McDowell, J. Mech. Phys. Solids **60**, 471 (2012).
[24] See Supplemental Material at http://link.aps.org/supplemental/10.1103/PhysRevMaterials.2.053602 for Movies 1 and 2.
[25] R. A. Gordon, Colleg. Math. J. **39**, 212 (2008).